01 Nov 1997

# Quantifying EMI Resulting from Finite-Impedance Reference Planes

David M. Hockanson

James L. Drewniak
*Missouri University of Science and Technology*, drewniak@mst.edu

Todd H. Hubing
*Missouri University of Science and Technology*

Thomas Van Doren
*Missouri University of Science and Technology*, vandoren@mst.edu

*et. al. For a complete list of authors, see https://scholarsmine.mst.edu/ele_comeng_facwork/1845*



## Recommended Citation

D. M. Hockanson et al., "Quantifying EMI Resulting from Finite-Impedance Reference Planes," *IEEE Transactions on Electromagnetic Compatibility*, vol. 39, no. 4, pp. 286-297, Institute of Electrical and Electronics Engineers (IEEE), Nov 1997.
The definitive version is available at https://doi.org/10.1109/15.649814

# Quantifying EMI Resulting from Finite-Impedance Reference Planes

David M. Hockanson, *Student Member, IEEE*, James L. Drewniak, *Member, IEEE*, Todd H. Hubing, *Senior Member, IEEE*, Thomas P. Van Doren, *Senior Member, IEEE*, Fei Sha, *Member, IEEE*, Cheung-Wei Lam, and Lawrence Rubin

***Abstract*—Parasitic inductance in printed circuit board (PCB) geometries can detrimentally impact the electromagnetic interference (EMI) performance and signal integrity of high-speed digital designs. This paper identifies and quantifies the parameters that affect the inductance of some typical PCB geometries. Closed-form expressions are provided for estimating the inductances of simple trace and ground plane configurations.**

***Index Terms*—Electromagnetic coupling, electromagnetic interference, inductance**

## I. Introduction

THE parasitic inductance, capacitance, and resistance of traces, vias, and planes on a printed circuit board (PCB) are important at high frequencies for modeling electromagnetic interference (EMI) and susceptibility processes. These parasitics comprise the effective noise source mechanism and coupling path of an integrated circuit (IC) source to an unintentional "antenna," which can result in an EMI or susceptibility problem. Parasitic inductance in PCB geometries is often the most difficult parameter to quantify. The concepts of inductance and partial inductance play a key role in PCB modeling. The inductance of the signal path is an important parameter in high-speed signal integrity calculations. Delta-I noise modeling, crosstalk calculations, and common-mode noise-source identification all rely on good estimates of the inductance associated with traces, vias, and signal return paths on PCB's.

Equivalent circuit models of EMI processes at the board level for geometries known to lead to problems that exceed regulatory limits are desirable at the design stage for estimating radiated emissions. A useful model includes an effective noise source, and the parasitics (inductance, capacitance, and resistance) that comprise the coupling path of the noise-source to the EMI antenna. This equivalent circuit can then be used together with a known or suspected EMI antenna and a full-wave solution of Maxwell's equations to estimate radiation.

Manuscript received October 21, 1996; revised July 28, 1997. This paper was supported in part by Fischer Custom Communications, NSF Graduate Fellowship (DMH), General Motors, and Allison Transmission.

D. M. Hockanson, J. L. Drewniak, T. H. Hubing, and T. P. Van Doren are with the Department of Electrical Engineering, Electromagnetic Compatibility Laboratory, University of Missouri, Rolla, MO 65401 USA.

F. Sha is with Northern Jaotong University, EMC Research Section, Beijing 100044, China.

C.-W. Lam and L. Rubin are with Viewlogic Systems, Inc. Camarillo, CA 93010 USA.

Publisher Item Identifier S 0018-9375(97)08419-6.

One noise-source mechanism results from signal currents returning through reference structures with finite impedance. This mechanism has previously been denoted *current-driven* [1]. In an equivalent circuit representation, the differential-mode signal current returning to its source results in a "voltage drop" across the finite impedance of the signal return. This potential difference can then drive two portions of the extended ground against each other as a dipole-type antenna leading to an EMI problem. The extended ground structures that form a dipole-type antenna can include reference planes on the PCB, attached cables, or a conducting chassis. In the approximate EMI antenna model, the signal trace is assumed to be negligible, and only those conductors carrying the majority of the common-mode current are included. An example of a current-driven noise source mechanism is a multi-signal flexible cable connecting two multilayer PCB's, with signal return routed only through a few lines [2]. The relatively high inductance associated with this signal return geometry results in a potential difference between the reference planes on the two PCB's. Any cables attached to the boards can then be driven against each other resulting in an EMI problem. Quantifying the inductance in signal return paths and reference planes, and developing an effective noise-voltage source from a return current through this inductance is important in constructing equivalent circuit models for modeling EMI noise source-mechanisms.

The inductance associated with a finite width PCB reference or ground plane that results in an EMI noise source is presented in this paper. The concept of partial inductance is briefly reviewed to compare and contrast the approach presented herein to previous work. Analytical expressions for the partial inductance of a trace over a ground plane, and partial inductance of a finite-width ground-plane are given. Measurements are presented for several cases of plane width and trace height above the ground plane to corroborate the analytical result for the variation of the partial inductance of a finite-width plane with plane width and trace height. The experimental and analytical results, in general, agree well.

## II. Partial Inductance Concept

The inductance of a closed loop (or mutual inductance of two closed loops) is defined as a ratio of the total magnetic flux that couples a closed path $i$ to the amplitude of the current in path $j$ that is the source of the magnetic flux

$$L_{ij} \equiv \frac{\Psi_i}{I_j} \text{ (Henries)}. \tag{1}$$

For a wire loop, the inductance is a function of the loop geometry as well as the shape and dimensions of the conductor. Although inductance is defined only for complete loops, it is often advantageous in developing equivalent circuits to assign *partial inductance* values to sections of a current loop [3]. This concept is useful in determining the effect of a particular segment on the overall inductance of a current path. For example, lowering the overall inductance of a particular geometry can be best accomplished by focusing attention on the segments of the path with the greatest partial inductance. The concept of partial inductance is also useful for estimating the voltage "dropped" across part of a circuit due to a current through a portion of a conductive path.

A useful definition for partial inductance in a closed path with $n$ segments is

$$L_{\text{total}} = L_{p1} + L_{p2} + \cdots + L_{pn} \tag{2}$$

where $L_{pi}$ is the partial inductance of the $i$th segment, and $L_{\text{total}}$ is the ratio of the total flux coupling the loop to the current in the loop. The current in each segment of the loop is equal, i.e., all current is conduction current. One definition for the partial inductance of the $i$th segment is the net flux that wraps the $i$th segment, divided by the current in Segment $i$. Since lines of magnetic flux are closed, the flux that wraps Segment $i$ and couples the loop is equal to the quantity of flux that couples the current Segment $i$ to infinity, i.e.,

$$L_{pi} = \frac{\Psi_i}{I} = \frac{\text{net flux coupling Segment } i \text{ to infinity}}{\text{amplitude of current in Segment } i}. \tag{3}$$

The magnetic vector potential $\vec{\boldsymbol{A}}$ is related to the magnetic field $\vec{\boldsymbol{H}}$ by $\vec{\boldsymbol{H}} \equiv (1/\mu)\nabla \times \vec{\boldsymbol{A}}$. Employing Stoke's theorem, the flux can be written in terms of a line integral [4]

$$\Psi = \mu \iint_S \vec{\boldsymbol{H}} \cdot \vec{\boldsymbol{ds}} = \iint_S (\nabla \times \vec{\boldsymbol{A}}) \cdot \vec{\boldsymbol{ds}} = \oint_L \vec{\boldsymbol{A}} \cdot \vec{\boldsymbol{dl}} \tag{4-a}$$

and

$$\Psi_i = \int_{L_i} \vec{\boldsymbol{A}} \cdot \vec{\boldsymbol{dl}}. \tag{4-b}$$

It is important to note from (4-b) that the calculation of partial inductance for each segment still requires a knowledge of the entire current path for determining $\vec{\boldsymbol{A}}$. Therefore, the same wire segment located in two different loops will, in general, have a different partial inductance.

Ruehli developed a concept he denoted *self-partial inductance* that is defined for a given segment of a loop independent of the location or orientation of any other loop segment [5]. For a straight wire segment with a finite wire radius as shown in Fig. 1(a), a rectangular loop is defined that is bounded by the wire segment on one side and infinity on the other. Two lines perpendicular to the wire segment and extending from the ends of the segment to infinity form the other two sides of the loop. Ruehli defined the self-partial inductance as the ratio of the net flux passing through this loop to the current on the wire segment (in the absence of all other segments and currents). Ruehli also defined a *mutual-partial inductance* between two wire segments. The mutual-partial inductance

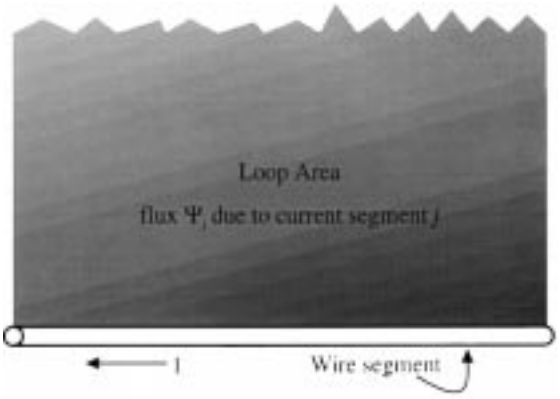


(a)

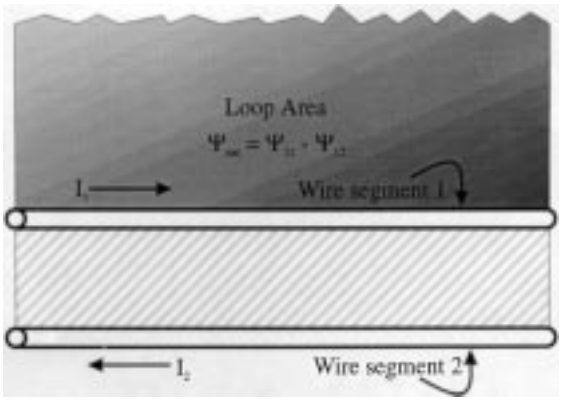


(b)

Fig. 1. Loop area used to define (a) self-partial inductance, (b) mutual-partial inductance, and net partial inductance.

$L_{ij}$ is the net flux produced by a current Segment $j$ that passes through the loop coupling Segment $i$ to infinity divided by $I_j$. For example, $L_{12} = \Psi_{12}/I_2$ as shown in Fig. 4(b). For two identical parallel segments, the partial inductance $L_{p_1} = L_{11} - L_{12}$ (i.e., the self-partial inductance minus the mutual-partial inductance) is equal to the total flux coupling the loop (between the two conductors) due to Segment 1, divided by the current in Segment 1 as seen in Fig. 4(b). In general, the partial inductance of a Segment $i$ can be defined as the self-partial inductance plus or minus the mutual-partial inductances between Segment $i$ and all other loop segments, i.e., [5]

$$L_{pi} = L_{ii} \pm \sum_{\substack{j=1 \\ j \neq i}}^{n} L_{ij}. \tag{5}$$

The sign of the mutual-partial inductance is determined by the relative orientation of the current on the two segments. If the flux from both segments passes through the infinite rectangular loop area in the same direction, the sign is positive. For segments with current flowing in opposite directions as shown in Fig. 4(b), the sign is negative. Ruehli's approach to partial inductance is very general. Ruehli *et al*. have successfully developed the partial element equivalent circuit (PEEC) method using the self- and mutual-partial inductance concepts for analyzing complicated geometries [6]–[8]. In addition to its generality, an advantage to Ruehli's formulation

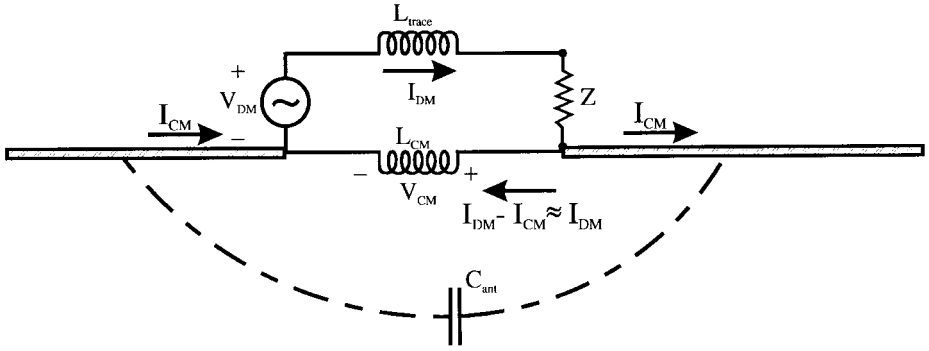


Fig. 2. Schematic drawing showing the physics of a current-driven noise-source mechanism.

is that the resulting equivalent circuit model incorporates the mutual interactions among elements. From an intuitive viewpoint this result is desirable. The approach taken herein employs Ruehli's fundamental concepts (the physics must be the same), but differs in the manner that portions of flux are assigned to parameters in an equivalent circuit model. The approach is not as general as Ruehli's, and is employed primarily to facilitate EMI noise source calculations from analytical expressions, and straight-forward comparisons with experimental results. An advantage of the approach pursued herein is that analytical expressions can be obtained for some geometries of particular interest for EMI noise source modeling, such as the partial inductance of a finite-width ground plane. Analytical expressions facilitate equivalent circuit modeling of EMI processes, and quick calculations. The approach is equivalent to Ruehli's, but does not involve the intermediate step of calculating any *self-* or *mutual-partial* inductances for segments of the conduction current path. The disadvantage is that a closed form expression may not be obtainable for all geometries of interest. Further, while the approach is intended for EMI calculations, Ruehli's approach is more satisfactory for signal integrity investigations.

## III. Common-Mode Inductance

Current-driven noise-source mechanisms in printed-circuit designs are a consequence of high-frequency currents returning through "ground" structures of finite impedance [1]. Flux wraps around ground planes of finite dimension causing common-mode current to flow. Magnetic flux, or the storage of magnetic energy can be modeled schematically as a partial inductance. The resulting voltage drop can drive two portions of an extended conductor against each other as an EMI antenna. The EMI noise-source for a current-driven mechanism may be defined as $V_{CM} \approx L_{CM}(d/dt)I_{DM}$ as shown in Fig. 2, where $L_{CM}$ denotes the "common-mode inductance," which here is the partial inductance of the signal return or ground structure. Traces over finite ground planes in PCB geometries can result in a voltage drop along the plane which may lead to common-mode radiation. Approximating the common-mode inductance can aid in predicting potential common-mode radiation problems in the design stage. Hoer *et al*. have developed formulas based on Neumann's formula for general rectangular geometries [9]. The formulas presented are for uniform current distributions over the conductors, and are complex. For nonuniform current distributions the conductor must be broken into smaller parts which may be modeled with a uniform current distribution and then the interaction between all elements must be analyzed. This approach (like Ruehli's) is complicated, but yields accurate results when numerically analyzed. Leferink has compiled a table of relatively simple expressions for calculating the partial inductance of various geometries [10], and gives a brief description of the methods of derivation. The reader is directed by Leferink to the references for a more thorough investigation. Leferink tabulates several partial inductance formulas for reference planes in trace-ground plane geometries. Expressions for several geometries vary as $\ln(h/w)$, where $h$ is the height of the trace over the reference plane and $w$ is the width of the reference plane. Two of Leferink's tabulated formulas vary as $h/w$ [11], [12]. Hubing *et al*. developed an expression varying as $h/w$ for the partial inductance of a plane in a trace over a finite ground plane geometry by assuming the current in the "tails" of the distribution of an infinite plane is redistributed over the finite plane uniformly [11]. Van Houten *et al*. developed an expression varying as $h/w$ for the transfer impedance between the voltage along a finite width plane and the current in the plane [12]. An $h/w$ variation of the partial inductance for a finite-width plane is derived here and experimentally verified. The singularity in the current at the edges of the plane is incorporated for the work presented herein, and, as a result, the constant coefficient associated with the $h/w$ expression differs from those tabulated by Leferink.

### A. Trace Over an Infinite Ground Plane

It is desirable in developing equivalent circuit models for noise sources to decompose the inductance of a trace over a finite width ground plane into a partial inductance of the signal trace, and the ground plane. For signal integrity calculations this decomposition is possibly unnecessary, however, for EMI noise-source modeling it is essential. The total inductance is the total flux linking the loop formed by the trace over the ground plane. The net flux coupled to infinity above the trace is associated with the partial inductance of the trace, and that coupled to infinity below the ground plane with the plane.

The partial inductance of a trace over an infinite ground plane is considered first because the results are needed in

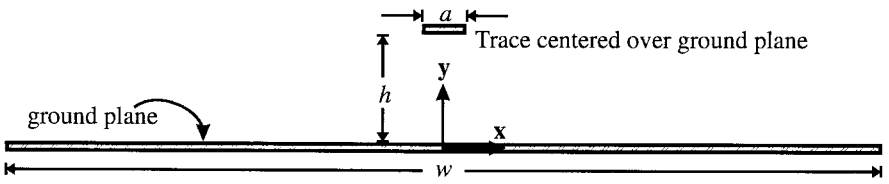


Fig. 3. Narrow trace centered above a plane.

determining the partial inductance of a finite ground plane. The trace centered over a ground plane is shown in Fig. 3. Assuming the trace is narrow, the current on the trace can be approximated by a uniform distribution

$$\vec{J}_{\text{trace}}(x) = \hat{z}\frac{I}{a}\delta(y-h)\Pi\left(\frac{x}{a}\right) \tag{6}$$

where $\Pi(x/a)$ is a spatial unit pulse of width $a$ centered at $x = 0$. The thickness of the strip is neglected. The magnetic vector potential $\vec{A}$ produced by $\vec{J}_{\text{trace}}(x)$ for this two-dimensional (2-D) case is

$$\vec{A}_{\text{trace}}(x,y) = -\hat{z}\frac{\mu I}{4a\pi}\int_{-(a/2)}^{+(a/2)} \ln\left[(x-x')^2+(y-h)^2\right]dx' \tag{7}$$

where the 2-D static Green's function $G(\vec{r}, \vec{r}') = (1/4\pi)\ln[(x-x')^2 + (y-y')^2]$ is used. If the plane below the trace is infinite ($w \to \infty$), image theory can be employed to determine the total magnetic vector potential for $y \geq 0$ as

$$\vec{A}_{\text{total}_{(w=\infty)}}(x,y) = -\hat{z}\frac{\mu I}{4a\pi}\int_{-(a/2)}^{+(a/2)} \{\ln\left[(x-x')^2+(y-h)^2\right] - \ln\left[(x-x')^2+(y+h)^2\right]\}dx'. \tag{8}$$

The partial inductance of the trace is the net total flux coupled from the trace to infinity ($y \to \infty$), as indicated in Fig. 4. The magnetic flux wrapping the trace or ground plane for the general case of finite ground plane width, can be calculated by evaluating the line integral of the magnetic vector potential as in (4-a), and the partial inductance calculated by dividing the flux by the current. The path of the line integral for the partial inductance calculation is the rectangle that extends to infinity with a normal in the $\hat{x}$ direction as shown in Fig. 4. The depth of the rectangle is simply $dz$, because the flux per unit length is the parameter of interest. Since the magnetic vector potential is always parallel to the current, only the $\hat{z}$ component of the magnetic vector potential is nonzero. Further, the value of $\vec{A}$ is zero as $y \to \infty$. Then, $\oint_{C_\infty} \vec{A}\cdot\vec{dl}$ evaluated around the loop to infinity, which is the net flux coupling the trace, reduces to an integration of $\vec{A}$ only along the trace. Since per unit length partial inductance is being calculated, this is simply $A_z(0,h)$. The partial inductance of the trace is then determined from the total magnetic vector potential at the center of the trace divided by the current I. Integrating (8) for $(x,y) = (0,h)$ and dividing by I, the partial inductance of a trace located over an infinite ground plane is

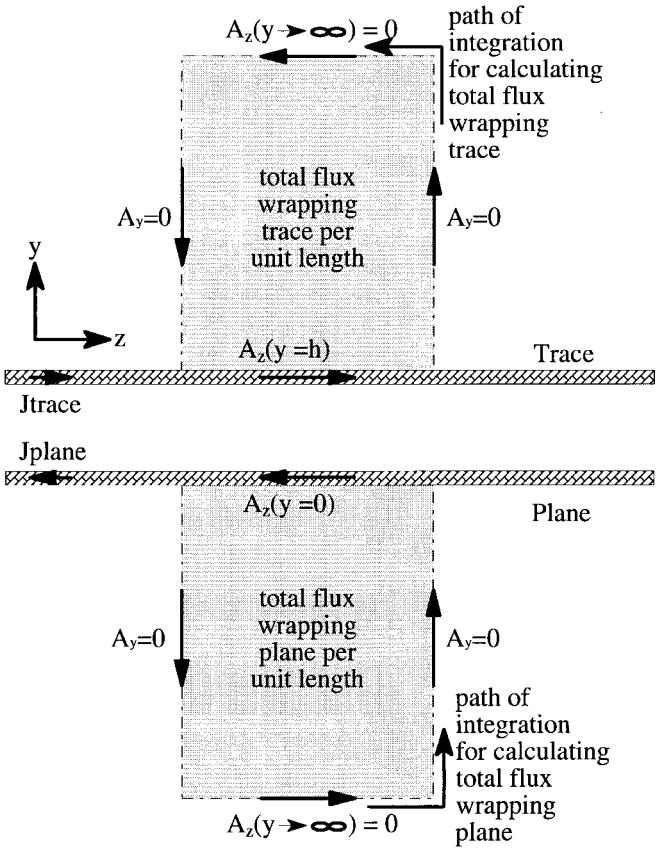


Fig. 4. Integration paths for determining the flux per unit length wrapping the trace and plane, respectively.

$$L^{\text{partial}}_{\text{trace}_{(w=\infty)}} = \frac{\mu}{2\pi}\left[\ln\sqrt{1+\left(\frac{4h}{a}\right)^2} + \frac{4h}{a}\tan^{-1}\left(\frac{a}{4h}\right)\right]\left(\frac{\text{H}}{\text{m}}\right). \tag{9}$$

Similarly, the partial inductance of the infinite plane can be determined by evaluating the magnetic vector potential at the origin. As a result, the partial inductance of the ground plane is zero, i.e.,

$$L^{\text{partial}}_{\text{plane}_{(w=\infty)}} = 0. \tag{10}$$

The partial inductance of the ground plane is expected to be zero because no magnetic flux lines can "wrap" around a plane of infinite extent. The total inductance per unit length associated with a trace over an infinite plane is then equal to the partial inductance of the trace. Conformal mapping has been previously used to approximate the transmission line

parameters of a microstrip line. Using conformal mapping, the inductance per unit length is given by [13]

$$L_{\text{microstrip}} \approx \begin{cases} \dfrac{\mu}{2\pi}\ln\left(\dfrac{8h}{a}+\dfrac{a}{4h}\right) \\ \qquad \dfrac{a}{h} \le 1 \\ \mu\left[\dfrac{a}{h}+1.393+0.667\ln\left(\dfrac{a}{h}+1.444\right)\right] \\ \qquad \dfrac{a}{h} \ge 1. \end{cases} \tag{11}$$

Equations (9) and (11) do not appear similar, however both equations can be approximated for the extreme cases as

$$L_{\text{microstrip}} \approx \begin{cases} \mu\dfrac{h}{a} & a \gg h \\ \dfrac{\mu}{2\pi}\ln\left(\dfrac{4h}{a}\right) & h \gg a. \end{cases} \tag{12}$$

The current distribution on the infinite plane is obtained from the magnetic vector potential in (8) as

$$\begin{aligned} &\vec{J}_{\text{plate}_{(w=\infty)}}(x) \\ &\quad = \frac{1}{\mu}\hat{y}\times\nabla\times\vec{A}_{\text{total}_{(w=\infty)}}(x,0) \\ &\quad = -\hat{z}\frac{I}{a\pi}\left[\tan^{-1}\left(\frac{x+\frac{a}{2}}{h}\right)-\tan^{-1}\left(\frac{x-\frac{a}{2}}{h}\right)\right]. \end{aligned} \tag{13}$$

Therefore the total magnetic vector potential for $y \ge 0$ with the return current on the infinite ground plane is

$$\begin{aligned} &\vec{A}_{\text{total}_{(w=\infty)}}(x,y) \\ &\quad = \vec{A}_{\text{trace}}(x,y)+\hat{z}\frac{\mu I}{4a\pi^2}\int_{-\infty}^{+\infty} \\ &\qquad \cdot\left[\tan^{-1}\left(\frac{x'+\frac{a}{2}}{h}\right)-\tan^{-1}\left(\frac{x'-\frac{a}{2}}{h}\right)\right] \\ &\qquad \cdot\ln\left[(x-x')^2+y^2\right]dx' \end{aligned} \tag{14}$$

where the second (integral) term is the contribution due to the current on the plane. This expression will be used in the following section to determine the partial inductance of a finite width plane that results in an EMI noise-source.

### *B. Trace Over a Finite Ground Plane*

Flux lines wrapping around a plane of finite dimension give rise to a partial inductance of the plane. A current through this partial inductance results in an EMI noise-source that can drive two portions of an extended conductor against each other leading to common-mode radiation as depicted in Fig. 2. The amount of flux that encircles the plane is small compared to the total flux coupling the trace-plane loop. Therefore, as long as the plane width is much greater than the distance between the trace and plane, the total inductance will not be significantly changed by considering the finite extent of the plane. The current density in (13) extends to infinity. The current beyond $w/2$ for the infinite plane must be redistributed over the plane of width $w$ for the finite case. Flux lines wrap around the finite plane as shown in Fig. 5(a). The flux lines are very dense at the edges of the plate indicating a high current density. The

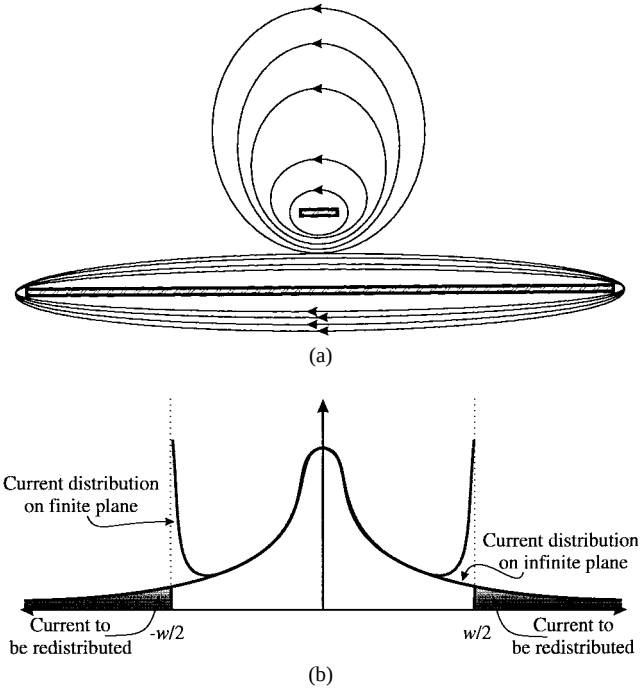


Fig. 5. (a) Flux lines wrapping around a trace and a finite plane. (b) Current distribution on a finite and an infinite plane.

current under the shaded region of Fig. 5(b) should then be redistributed in such a fashion that the current density is very large at the edges of the plane. One current model with the desired edge singularities is

$$\begin{aligned} &\vec{J}_{\text{plate}_{(w<\infty)}}(x) \\ &\quad = -\hat{z}\frac{I}{\pi}\Pi\left(\frac{x}{w}\right)\left\{\frac{1}{a}\left[\tan^{-1}\left(\frac{x+\frac{a}{2}}{h}\right)\right.\right. \\ &\qquad \left.\left.-\tan^{-1}\left(\frac{x-\frac{a}{2}}{h}\right)\right]+\frac{4h}{w\pi}\frac{1}{\sqrt{\left(\frac{w}{2}\right)^2-x^2}}\right\} \end{aligned} \tag{15}$$

where integration over the plate yields a total current $I$, (assuming $w \gg h, a$). The second term of the current-density expression (the redistributed portion) was chosen because it has the desired edge singularities and is integrable.

The total magnetic vector potential for a finite plane using the current distribution of (15) is

$$\begin{aligned} &\vec{A}_{\text{total}_{(w<\infty)}}(x,y) \\ &\quad = \vec{A}_{\text{trace}}(x,y)+\hat{z}\frac{\mu I}{4a\pi^2}\int_{-(w/2)}^{+(w/2)} \\ &\qquad \cdot\left[\tan^{-1}\left(\frac{x'+\frac{a}{2}}{h}\right)-\tan^{-1}\left(\frac{x'-\frac{a}{2}}{h}\right)\right] \\ &\qquad \cdot\ln\left[(x-x')^2+y^2\right]dx'+\hat{z}\frac{\mu I h}{w\pi^3}\int_{-(w/2)}^{+(w/2)} \\ &\qquad \cdot\frac{\ln\left[(x-x')^2+y^2\right]}{\sqrt{\left(\frac{w}{2}\right)^2-x^2}}dx'. \end{aligned} \tag{16}$$

For partial inductance calculations, $\vec{A}$ is integrated in the $x = 0$ plane, and

$$\begin{aligned}\vec{A}_{\text{total}_{(w<\infty)}}(0,y) &= \vec{A}_{\text{trace}}(0,y) + \hat{z}\frac{\mu I}{4a\pi^2}\int_{-\infty}^{+\infty} \cdot\left[\tan^{-1}\left(\frac{x'+\frac{a}{2}}{h}\right)-\tan^{-1}\left(\frac{x'-\frac{a}{2}}{h}\right)\right] \cdot\ln[x'^2+y^2]\,dx' - \hat{z}\frac{\mu I}{4a\pi^2}\int_{-\infty}^{-(w/2)} \cdot\left[\tan^{-1}\left(\frac{x'+\frac{a}{2}}{h}\right)-\tan^{-1}\left(\frac{x'-\frac{a}{2}}{h}\right)\right] \cdot\ln[x'^2+y^2]\,dx' - \hat{z}\frac{\mu I}{4a\pi^2}\int_{+(w/2)}^{+\infty} \cdot\left[\tan^{-1}\left(\frac{x'+\frac{a}{2}}{h}\right)-\tan^{-1}\left(\frac{x'-\frac{a}{2}}{h}\right)\right] \cdot\ln[x'^2+y^2]\,dx' + \hat{z}2\frac{\mu I h}{w\pi^3}\int_{0}^{+(w/2)} \cdot\frac{\ln[x'^2+y^2]}{\sqrt{\left(\frac{w}{2}\right)^2-x'^2}}dx' \end{aligned} \tag{17}$$

where the first integral in (16) has been rewritten as the sum of three integrals, and $\vec{A}$ is evaluated at $x = 0$. Substituting (14) in (17), the magnetic vector potential at $x = 0$ is

$$\begin{aligned}\vec{A}_{\text{total}_{(w<\infty)}}(0,y) &= \vec{A}_{\text{total}_{(w=\infty)}}(0,y) - \hat{z}\frac{\mu I}{2a\pi^2}\int_{w/2}^{\infty}\tan^{-1} \cdot\left(\frac{ha}{x'^2+h^2-\left(\frac{a}{2}\right)^2}\right)\ln(x'^2+y^2)\,dx' + \hat{z}\frac{\mu I 2h}{w\pi^2}\ln\left(\frac{|y|+\sqrt{y^2+\left(\frac{w}{2}\right)^2}}{2}\right). \end{aligned} \tag{18}$$

For $y \ll w/2$, which is the case of interest, the total magnetic vector potential is approximately

$$\vec{A}_{\text{total}_{(w<\infty)}}(0,y) \approx \vec{A}_{\text{total}_{(w=\infty)}}(0,y) - \hat{z}\frac{\mu I h}{\pi^2 w}2(\ln 2+1). \tag{19}$$

Since the trace-plane separation $h$ is assumed much smaller than $w/2$, the partial inductance of the trace and the plane can be determined using (19) by evaluating the magnetic vector potential at $y = h$, and $y = 0$, respectively, and dividing by the current $I$, i.e.,

$$\begin{aligned} L_{\substack{\text{partial}\\ \text{trace}_{(w<\infty)}}} &\approx L_{\substack{\text{partial}\\ \text{trace}_{(w=\infty)}}} - \frac{\mu}{\pi^2}\,\frac{h}{w}2(\ln 2+1) \\ &\approx L_{\substack{\text{partial}\\ \text{trace}_{(w=\infty)}}} \quad (\text{H/m}) \end{aligned} \tag{20}$$

$$L_{\substack{\text{partial}\\ \text{trace}_{(w<\infty)}}} \approx \frac{\mu}{\pi^2}\,\frac{h}{w}2(\ln 2+1) \approx 4\frac{h}{w} \quad (\text{nH/cm}) \tag{21}$$

where $L_{\substack{\text{partial}\\ \text{trace}_{(w=\infty)}}}$ is given by (9). The total inductance calculated is the same for both the case of the infinite ground plane and the finite plane. This results from the assumption that the plane width was much greater than the trace-plane separation. One consequence of the inductance results is that the signal integrity aspects of the trace-plane configuration are unaffected by changing the plane width (for planes with $w \gg h$). For example if the ground plane is wide with respect to the trace-plane separation, doubling the plane width has no discernable effect on the loop impedance for the signal current. However, doubling the plane width halves $L_{CM}$, and reduces the EMI noise-source driving common-mode radiation by 6 dB.

An upper bound for the common-mode inductance associated with the finite plane can be calculated by assuming the excess current is redistributed uniformly over the plate (see Fig. 5). The current distribution on the plate is then approximately

$$\begin{aligned}\vec{J}_{\text{plate}_{(w<\infty)}}(x) &= -\hat{z}\frac{I}{\pi}\Pi\left(\frac{x}{w}\right) \cdot\left\{\frac{1}{a}\left[\tan^{-1}\left(\frac{x+\frac{a}{2}}{h}\right)-\tan^{-1}\left(\frac{x-\frac{a}{2}}{h}\right)\right]+\frac{4h}{w^2}\right\} \end{aligned} \tag{22}$$

and the total magnetic vector potential in the $x = 0$ plane is

$$\begin{aligned}\vec{A}_{\text{total}_{(w<\infty)}}(0,y) &= \vec{A}_{\text{total}_{(w=\infty)}}(0,y) - \hat{z}\frac{2h\mu I}{w\pi^2}\left(\ln\frac{w}{2}+1\right) + \hat{z}\frac{\mu I h}{w^2\pi^2}\int_{-(w/2)}^{+(w/2)}\ln(x'^2+y^2)\,dx'. \end{aligned} \tag{23}$$

The partial inductance of the trace calculated from $\vec{A}_{\text{total}_{w<\infty}}(0,h)$ is virtually unchanged by the current redistribution, because the partial inductance of the plane is small compared to the partial inductance of the trace. The total inductance of the trace over a ground plane is still very nearly the partial-inductance of the trace. However, the total magnetic vector potential at the origin is

$$\vec{A}_{\text{total}_{(w<\infty)}}(0,0) = -\hat{z}4\frac{\mu I}{\pi^2}\,\frac{h}{w}. \tag{24}$$

Therefore, the partial inductance of the finite plane, or "common-mode" inductance is

$$L_{CM} = L_{\substack{\text{partial}\\ (w<\infty)}} \approx \frac{4\mu h}{\pi^2 w} \approx 5\frac{h}{w} \quad (\text{nH/cm}). \tag{25}$$

TABLE I
VALUES OF TOTAL INDUCTANCE CALCULATED ANALYTICALLY USING (9) AND (11), AND EXPERIMENTALLY USING THE DATA PROVIDED BY THE HP4291A IMPEDANCE ANALYZER FOR A TRACE 2 mm WIDE, 20 cm LONG, AND A HEIGHT $h$ ABOVE THE REFERENCE PLANE

| Total Inductance Results | | | | | |
|---|---|---|---|---|---|
| Height of trace above reference plane ($mm$) | Experimental Result ($nH$) | Analytical Result ($nH$) | % Difference | Conformal Mapping Result ($nH$) | % Difference |
| 1.65 | 86 | 88 | 2.3% | 77 | 10.5% |
| 3.3 | 115 | 116 | 0.8% | 104 | 9.5% |
| 6.6 | 144 | 143 | 0.7% | 131 | 9.0% |

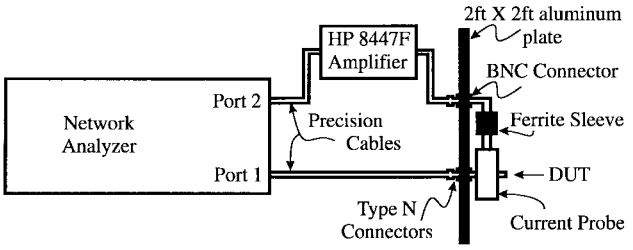


Fig. 6. Equipment configuration for determining the common-mode current generated on a cable using an HP8753C network analyzer.

The common-mode inductance expression resulting from a uniform current differs only slightly from the expression for a nonuniform current distribution. Either form should provide first order accuracy for predicting the level of the common-mode noise-source.

## IV. EXPERIMENTAL RESULTS

The effects of trace height and plane width on the common-mode noise-source due to the finite ground impedance were investigated experimentally. An HP8753C network analyzer was employed for $|S_{21}|$ measurements. The experimental configuration is illustrated schematically in Fig. 6. Port 1 of the network analyzer was the driving source for the circuit, and the output of a common-mode current probe was input to Port 2. An HP8447F RF Amplifier (28 dB amplification: 9 kHz–50 MHz) was used to increase the dynamic range of the measurements. The effective source impedance for the circuit was the 50 $\Omega$ impedance of the network analyzer. A $2' \times 2'$ square aluminum plate was used in all the measurement procedures in order to obtain a sufficiently large common-mode current to measure, and to provide a test environment for making repeatable measurements. The measured common-mode current was not a function of the network analyzer cable dressing when the aluminum plate was employed. The common-mode current was measured using a Fischer F-33-1 (200 kHz–250 MHz) current probe. A ferrite sleeve (200 $\Omega$ at 100 MHz) was employed to reduce parasitic coupling to the current probe. The transfer impedances of the current probe and the amplifier were included in the calibration procedures using the error correction capabilities of the HP8753C network analyzer.

The experimental test device is shown in Fig. 7. A 0.085 in a semi-rigid coaxial cable was electrically well connected to the bottom of the large ground plane. The center conductor was extended through the plane (from the bottom side of the plane), and connected to a trace on the top side of the test board. The 20 cm trace was shorted to the plane at the load

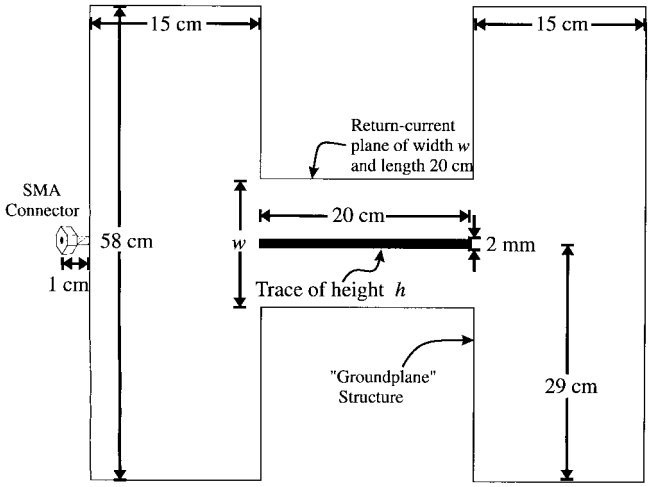


Fig. 7. Test configuration for measuring the affect of trace height and plane width on the common-mode inductance.

end resulting in a rectangular loop of dimensions 20 cm $\times$ $h$, where $h$ was the trace height above the ground plane. The trace was 2 mm wide. The ground plane regions near the source and shorted ends were extended to a width of 58 cm so the common-mode noise-source ($\approx j\omega I_{DM} L_{CM}$) would be dominated by the flux wrapping around the plane of width $w$ beneath the signal trace. First, the total inductance of the loop composed of the 2 mm wide trace over the reference plane and terminated in a short circuit was calculated using (9). The calculated inductance values were compared with the values determined from input impedance measurements with an HP4291A Impedance Analyzer, as an initial check on the theory. The calculated and experimentally determined inductance values, and percent difference are shown in Table I. The analytical and experimental values in general agree well. The analytical results calculated using (9) agree with the experimental results within a few percent, however, the analytical results using (11) predict an inductance that is typically 10% less than the experimental results.

### A. Partial Inductance Variation with $w$ and $h$

The common-mode noise-source for the geometry in Fig. 7 is current-driven [1], and is the potential difference generated by the signal return current through the finite impedance plane of width $w$ below the trace. Below the antenna resonance frequencies the common-mode current measured with the current-probe is [1]

$$|I_{CM}| \approx \kappa \omega^2 L_{CM} C_{\text{ant}} \frac{V_{DM}}{|Z_{in}|} \tag{26}$$

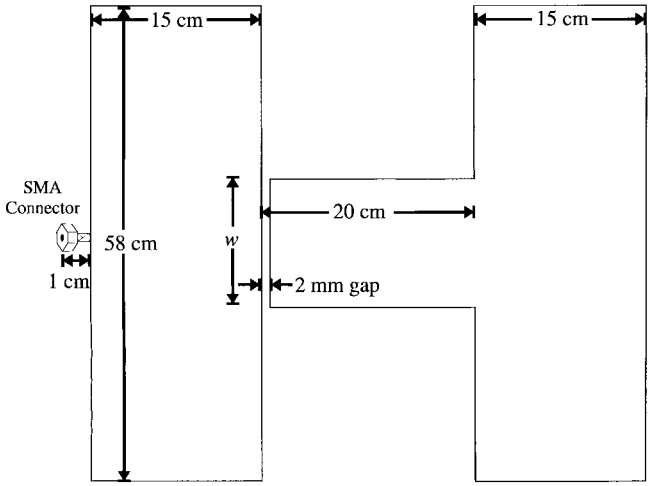


Fig. 8. Test configuration for measuring the antenna input impedance with respect to changes in plane width.

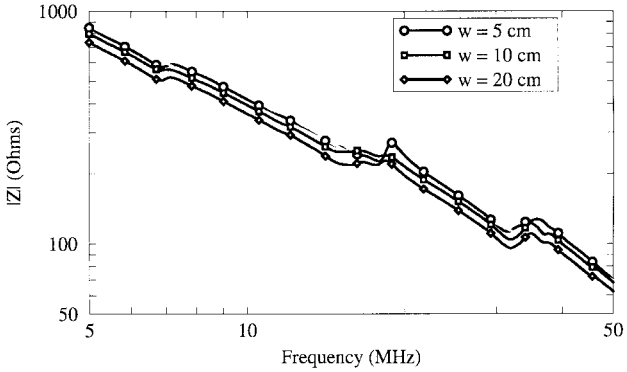


Fig. 9. Measured input impedance results with the HP4291A Impedance/Material Analyzer for the EMI antenna configuration of Fig. 8 with $w = 5$, $w = 10$, and $w = 20$ cm.

where $L_{CM}$ is the reference plane partial inductance given by (21), $Z_{\text{ant}} = j\omega C_{\text{ant}}$ is the EMI antenna impedance (which is capacitive below resonance), $|Z_{in}|$ is the input impedance seen at the source terminals, and $0 \leq \kappa \leq 1$ is a constant to indicate that the current probe is not located at the effective feed point of the EMI antenna. It is assumed that $Z_{\text{in}} = 50 + j\omega L_{\text{total}}$, and that the antenna impedance does not significantly affect the differential-mode drive current. The signal circuit input impedance measurements corroborate this assumption. The EMI antenna in this case is the extended ground structure with the two pieces on each side of the necked region of width $w$ comprising two portions of a "dipole-type" antenna. The aluminum plate connected to one side and the 20 cm length of the signal return plane over which the common-mode noise-source is distributed are also portions of the antenna. The differential-mode current is $V_{DM}/Z_{\text{in}}$. Assuming a 50 $\Omega$ source impedance, $Z_{\text{in}} = 50 + j\omega L_{\text{total}}$, where $L_{\text{total}}$ is the total inductance of the signal and return loop. At the measurement frequencies the test configuration is electrically short so that the trace can be treated as a lumped element.

In order to test (21), it is essential to either keep the antenna input impedance constant, or adequately account for it in the measurements. The test configuration depicted in Fig. 7 has an antenna input impedance that varies with the width of the return-current plane. The noise-source is distributed over the length of the reference plane beneath the trace, which makes accurate experimental investigations of the antenna input impedance difficult. However, the antenna input impedance can be approximated by measuring the input impedance at a defined pair of terminals using the HP4291A Impedance/Material Analyzer (1 MHz–1.8 GHz). The geometry for this experiment is shown in Fig. 8. The return-current plane of width $w$ is separated at the source end from the rest of the ground plane by a 2 mm wide gap. The trace was removed and the center conductor of the 0.085 in coaxial cable was connected to the return-current plane of width $w$ across the gap. The test device was connected to the experimental configuration of Fig. 6 with Port 1 connected to the Impedance Analyzer and Port 2 (with the current probe in place) terminated in 50 $\Omega$. Fig. 9 shows the results for $w = 5$, 10, and 20 cm. Small resonances were measured at approximately 7, 20, and 35 MHz. The three resonances may be associated with the unusual geometry of the test device, but because of the relatively low frequencies they are more likely associated with the parasitics of the experimental setup. The curves generally decrease at approximately 20 dB/decade as expected for a predominantly capacitive antenna input impedance, although the resonances perturb the slope slightly. Using the data at 5 MHz, the capacitance of the effective EMI antenna increases approximately 0.5 dB when the width of the return-current plane is doubled.

The common-mode current driven by the finite impedance return plane noise source shown in Fig. 7 was measured for $w = 5$, 10, and 20 cm with $h = 1.65$ mm. The input impedance $Z_{\text{in}}$ at Port 1 (looking into the 20 cm signal trace terminated in a short) was measured with an HP4291A Impedance/Material Analyzer. No discernable difference was measured in the input impedance for $w = 5$, 10, and 20 cm, and the magnitude of the input impedance was less than 50 $\Omega$ for frequencies below 50 MHz. Consequently, the drive current ($I_{DM} = V_{DM}/Z_{\text{in}}$) was the same for all three geometries. Further, since $|Z_{\text{in}}|$ was approximately 50, 51, and 57 $\Omega$ at 5, 20, and 50 MHz, respectively; the drive current $I_{DM}$ was relatively constant over the measured frequency range. The common-mode current at the effective source terminals of the antenna (where the triangular current distribution peaks) is then $|I_{CM}| \approx \omega^2 L_{CM} C_{\text{ant}} |V_{DM}/Z_{\text{in}}|$. With the transfer-impedances of the current-probe and amplifier taken into account in the calibration procedure, the voltage at Port 2 is

$$V_2^- = 50\kappa \frac{I_{CM}}{2} \tag{27}$$

where $\kappa$ is a proportionality constant because the common-mode current is not measured at the effective antenna terminals. The factor of two shown in the denominator results from the calibration procedure. The magnitude of $S_{21}$ is

$$|S_{21}| = \left|\frac{V_2^-}{V_1^+}\right| \approx \left|\frac{50\kappa I_{CM}}{V_{DM}}\right| \approx \kappa\omega^2 L_{CM} C_{\text{ant}} \frac{50}{|Z_{\text{in}}|} \tag{28}$$

where $V_1^+ = V_{DM}/2$, because the 50 $\Omega$ source impedance is matched to the characteristic impedance of the cables. $V_{DM}$ is

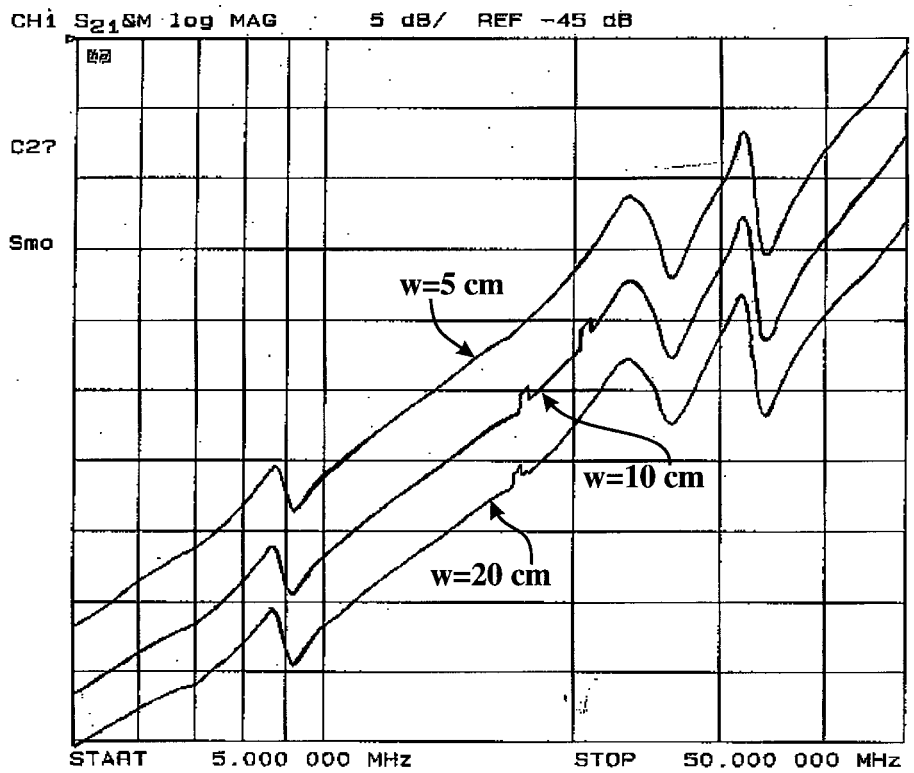


Fig. 10. Measured common-mode current for a return-current plane width of 5, 10, and 20 cm, and a trace height of $h = 1.65$ mm.

the RF source voltage of the network analyzer. Using (21), and considering the change in antenna capacitance as discussed above, $|S_{21}|$ increases by

$$20\log_{10}\left|\frac{S_{21}^{(w/2)}}{S_{21}^{w}}\right| \approx 20\log_{10}\frac{\frac{2h}{w}C_{\text{ant}}\left(\frac{w}{2}\right)}{\frac{h}{w}C_{\text{ant}}(w)} = 20\log_{10}2 - 20\log_{10}\frac{C_{\text{ant}}(w)}{C_{\text{ant}}\left(\frac{w}{2}\right)} \approx 5.5\ \text{dB} \tag{29}$$

when the return-current plane width was halved. Fig. 10 shows the experimental $|S_{21}|$ results for plane widths of $w = 5$, 10, and 20 cm with a trace height $h = 1.65$ mm. The measured increase in $|S_{21}|$ when the return-current plane width was halved was between 5 and 6 dB, with typical values approximately 5.5 dB. The increase in $|S_{21}|$ when the plane width was decreased from 20–10 cm was between 4 and 5 dB at lower frequencies (5–9 MHz), which may be a result of lower SNR at these frequencies. In general the data corroborates the theoretically expected results well. Approximating a best-fit line to the measured $|I_{CM}|$ between 5 and 20 MHz, the increase in frequency is very nearly 40 dB/decade as expected for a current-driven EMI source mechanism [1]. The small "pulses" in the data resulted from noise spikes that were smoothed with the averaging capabilities of the network analyzer. The resonances in the data at approximately 9, 25, and 33 MHz resulted from parasitic effects between the measurement configuration and the test board. The exact nature of the parasitics is unknown. The calibration features of the HP8753C account for the frequency response of the measurement setup, but not for the interactions of the setup with the test board.

The common-mode current was also measured for several heights of the trace above the return-current plane for a constant plane width of $w = 20$ cm. The input impedance $|Z_{\text{in}}|$ of the test configuration was measured at the feed point of the shorted signal trace with the HP4291A Impedance Analyzer for $h = 1.65$, 3.3, and 6.6 mm. The measured $|Z_{\text{in}}|$ at 20 MHz for $h = 1.65$, 3.3, and 6.6 mm was 52.2, 53.1, and 55.5 $\Omega$. As a result, the drive current $I_{DM}$ was approximately constant for the three different geometries, as well as approximately constant in frequency up to 20 MHz. At 50 MHz, the measured input impedance $|Z_{\text{in}}|$ was 67.3, 75.1, and 88.5 $\Omega$. Consequently, the signal drive current $I_{DM}$ was varying between 20 and 50 MHz. However, the parasitic resonances in this frequency range associated with the test configuration masked the effect of the increasing drive current on $I_{CM}$.

The antenna input impedance does not change with trace height, since the antenna is comprised of only the extended ground conductors, so $|S_{21}|$ should increase by 6 dB according to (21) when the trace height is doubled, i.e.,

$$20\log_{10}\left|\frac{S_{21}^{2h}}{S_{21}^{h}}\right| \approx 20\log_{10}\frac{\frac{2h}{w}C_{\text{ant}}}{\frac{h}{w}C_{\text{ant}}} = 20\log_{10}2 \approx 6.0\ \text{dB}. \tag{30}$$

Fig. 11 shows the $|S_{21}|$ results for $h = 1.65$, 3.3, and 6.6 mm. The difference in $|S_{21}|$ for frequencies below 9 MHz

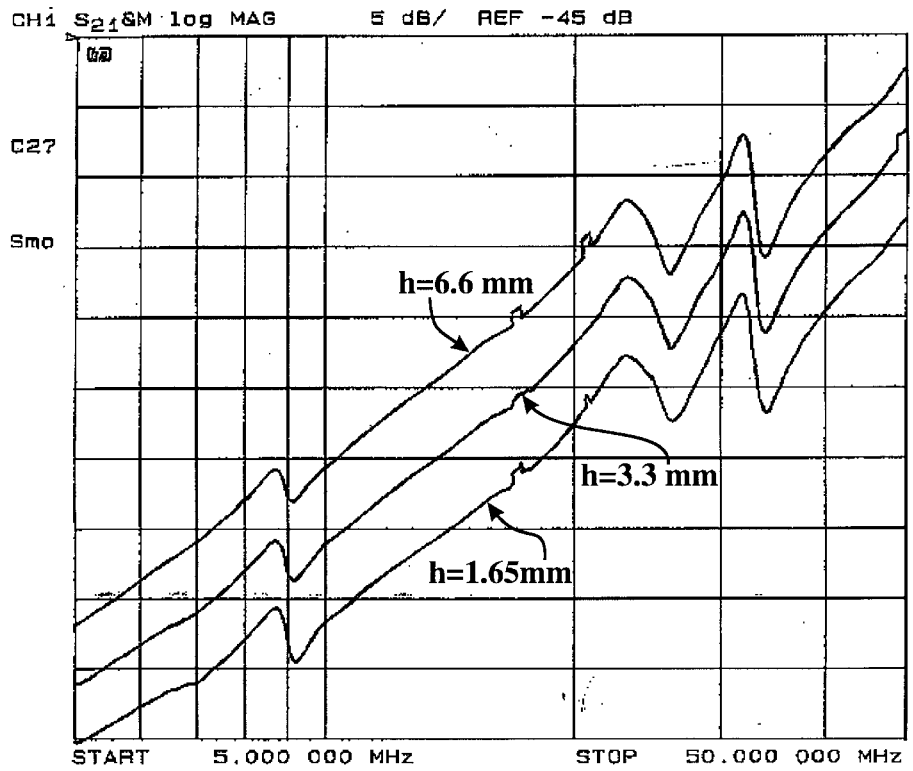


Fig. 11. Measured common-mode current for a trace height of 1.65, 3.3, and 6.6 mm, and a trace width of $w = 20$ cm.

is between 4 and 5 dB, and is lower than expected, because of a lower SNR than at higher frequencies. Above 10 MHz, differences are between 5.5 and 6 dB, supporting the analytical results of (21) for the $h/w$ variation. The analytical conclusion that the common-mode inductance is proportional to $h/w$ is further supported by the close correlation of Figs. 10 and 11. The trace curves for these two sets of results (five different cases) should be virtually identical because the ratio $h/w$ was changed by a factor of two in both the case where the width $w$ was changed, as well as when the height $h$ was changed. Slight discrepancies result from small changes in drive current and antenna impedance as the parameters $h$ and $w$ were changed.

The proportionality constant $\kappa$ is unknown and prevents direct calculation of $L_{CM}$ from the experimental data. When $L_{CM}$ is calculated using the the experimental data with $\kappa = 1$, the result is approximately one half of the analytical value (possibly indicating $\kappa = 0.5$). This factor of two occurs when calculating the experimental value of $L_{CM}$ using any of the three ratios of $h$ to $w$ for which data is available. The uniformity of the factor of two may indicate that the current distribution on the EMI antenna outside the source region does not change as $L_{CM}$ changes, rather only the EMI noise-source or the magnitude of the current distribution changes.

### *B. Partial Inductance Coefficient Evaluation*

A separate experiment was performed to investigate the coefficient $2(\mu/\pi^2)(\ln 2 + 1) \approx 4$(nH/cm) in the partial inductance expression. The test configuration of Fig. 7 was used with two different trace widths over a 5 cm wide reference plane. First, a 2 mm wide trace was centered over the reference plane. The common-mode current that results is given by (26). The data for a 2 mm trace was compared to that of a 5 cm wide trace centered over the reference plane with $h = 1.65$ mm and $w = 5$ cm.

A parallel plate transmission line of width $w$ and height $h$ has an inductance per unit length

$$L_{\|\text{plate}} = \mu \frac{h}{w} \quad (\text{H/cm}) \tag{31}$$

assuming $w \gg h$ [14]. Because the parallel plate transmission line has electrical symmetry, half of the magnetic flux wraps the trace conductor, and half of the flux wraps the reference plane. Therefore, the common-mode inductance $L_{CM}$ associated with the reference plane in the parallel plate transmission line geometry is half of the total loop inductance

$$L_{CM}^{\|\text{plate}} = \frac{\mu h}{2w}. \tag{32}$$

Assuming that the circuit input impedance ($\approx 50\ \Omega$) and antenna input impedance is the same for the two trace geometries, the difference in common-mode current is

$$\frac{I_{CM}^{\|\text{plate}}}{I_{CM}^{\text{microstrip}}} = \frac{L_{CM}^{\|\text{plate}}}{L_{CM}^{\text{microstrip}}} = \frac{\dfrac{\mu h}{2w}}{\dfrac{\mu h}{\pi^2 w}\, 2(\ln 2 + 1)} \approx 3.3 \text{ dB}. \tag{33}$$

The experimental results are shown in Fig. 12. A difference in the data for the two cases of 3–4 dB up to approximately 30 MHz supports the analytical expression for the common-mode inductance of the reference plane for the microstrip geometry. Above 30 MHz the difference increases slightly with frequency to approximately 5 dB at 50 MHz. The increase

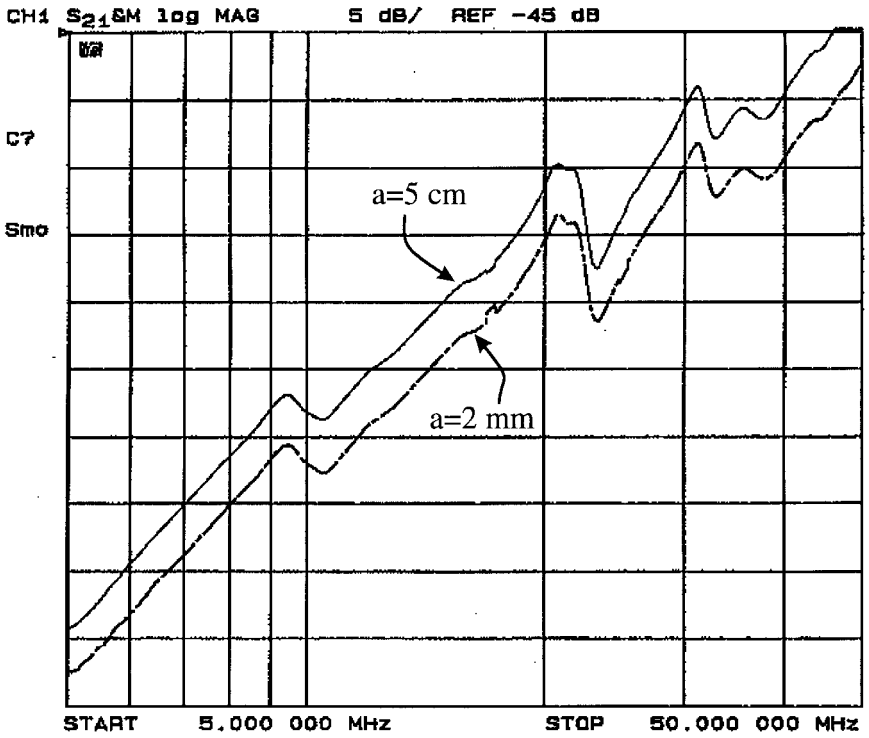


Fig. 12. Measured common-mode current for a trace height of 1.65 mm and a trace width of $w = 5$ cm for trace widths $a = 2$ mm and $a = 5$ cm.

is due to the low inductance of the parallel plate transmission line as compared to the microstrip geometry. Equation (33) assumes that the input impedance of the two circuit geometries is the same. However, the inductance of the circuit with a planar transmission line is approximately 8.3 nH; an order of magnitude less than the inductance of the microstrip loop. At 50 MHz the difference in input impedance is approximately 1.1 dB, which accounts for the discrepancy at the higher frequencies.

## V. Conclusion

Partial inductance concepts were reviewed to provide a clear understanding of the calculation and use of partial inductances. The partial inductance of a trace over a ground plane geometry was investigated analytically and experimentally. A closed form expression was derived for the total inductance of a trace centered over a ground plane, and these results used to obtain a simple closed-form expression for the partial inductance per unit length of the ground plane for a centered trace. The ground plane partial inductance may play a primary role as an EMI noise-source in radiation problems for high-speed systems. The partial inductance of the ground plane was found analytically to be directly proportional to the ratio $h/w$, where $h$ is the height of the trace over the ground plane and $w$ is the width of the ground plane. An experimental test configuration was designed to test the partial inductance dependence on $h$ and $w$. The experiments supported the dependence of $L_{CM}$ on $h$ and $w$. The constant associated with the partial inductance expression was verified by comparing the common-mode current generated with a microstrip geometry and a planar transmission line geometry. The critical observation was supported that by reducing the ratio $h/w$ a potentially problematic EMI noise-source may be diminished. One shortcoming of increasing the width of the ground plane to reduce the noise-source is the consequent reduction of the input impedance if the ground plane is a major portion of an EMI antenna. However, if the cables and chassis of a device are the principal pieces of the EMI antennas, it is probable that changes in ground plane width will not noticeably change the antenna input impedance.

## Acknowledgment

The authors would like to thank A. Ruehli for his helpful correspondence.

## References

[1] D. M. Hockanson, J. L. Drewniak, T. H. Hubing, T. P. Van Doren, F. Sha, and M. Wilhelm, "Investigation of fundamental EMI source mechanisms driving common-mode radiation from printed circuit boards with attached cables," *IEEE Trans. Electromag. Compat.*, vol. 38, June 1996.

[2] J. L. Drewniak, F. Sha, T. H. Hubing, T. P. Van Doren, and J. Shaw, "Diagnosing and modeling common-mode radiation from printed circuit boards with attached cables," in *Proc. 1995 IEEE Int. Symp. Electromag. Compat.*, Chicago, IL, Aug. 1995, pp. 465–470.

[3] H. W. Grover, *Inductance Calculations: Working Formulas and Tables*. New York: Dover, 1962.

[4] C. R. Paul, *Introduction to Electromagnetic Compatibility*. New York: Wiley, 1992.

[5] A. E. Ruehli, "Inductance calculations in a complex integrated circuit environment," *IBM J. Res. Develop.*, vol. 16, pp. 470–481, 1972.

[6] ——, "Equivalent circuit models for three-dimensional multiconductor systems," *IEEE Trans. Microwave Theory Tech.*, vol. MTT-22, pp. 216–221, Mar. 1974.

[7] A. Ruehli, U. Miekkala, A. Bellen, and H. Heeb, "Stable time domain solutions for EMC problems using PEEC circuit models," in *Proc. IEEE Int. Symp. Electromag. Compat.*, Chicago, IL, 1994, pp. 371–376.

[8] A. Ruehli, "Partial element equivalent circuit (PEEC) method and its application in the frequency and time domain," in *IEEE Int. Symp. Electromag. Compat.*, Santa Clara, CA, 1996, pp. 128–133.
[9] C. Hoer and C. Love, "Exact inductance equations for rectangular conductors with applications to more complicated geometries," *J. Res. National Bureau Standards—C. Engineering and Instrumentation*, vol. 69C, pp. 127–137, Apr.–June 1965.
[10] F. B. J. Leferink, "Inductance calculations: methods and equations," in *Proc. IEEE Int. Symp. Electromag. Compat.*, Atlanta, GA, 1995, pp. 16–22.
[11] T. H. Hubing, T. P. Van Doren, and J. L. Drewniak, "Identifying and quantifying printed circuit board inductance," in *Proc. IEEE Int. Symp. Electromag. Compat.*, Chicago, IL, 1994, pp. 205–208.
[12] M. A. Van Houten, E. J. M. Van Heesch, A. P. J. Van Deursen, R. G. Noij, J. N. A. M. Van Rooy, and P. C. T. Van der Laan, "General methods for protection of electronics against interference, tested in high-voltage substations," in *Proc. IEEE Int. Symp. Electromag. Compat.*, Zurich, Switzerland, 1989, pp. 429–434.
[13] D. M. Pozar, *Microwave Engineering.* Reading, MA: Addison-Wesley, 1990.
[14] S. V. Marshall, R. E. DuBroff, and G. G. Skitek, *Electromagnetic Concepts and Applications*, 4th ed., Upper Saddle River, NJ: Prentice-Hall, 1996.

**David M. Hockanson** (S'90), for a biography, see p. 232 of the August 1997 issue of THIS TRANSACTIONS.

**James L. Drewniak** (S'85–M'90), for a photograph and biograpy, see p. 155 of the May 1997 issue of this TRANSACTIONS.

**Todd H. Hubing** (S'82–M'82–SM'93), for a photograph and biograpy, see p. 155 of the May 1997 issue of this TRANSACTIONS.

**Thomas P. Van Doren** (M'58), for a photograph and biograpy, see p. 155 of the May 1997 issue of this TRANSACTIONS.

**Fei Sha** (M'91), for a biography, see this issue, p. 285.

**Cheung-Wei Lam** was born in Hong Kong, on March 5, 1965. He received the B.S. degree in electronics from the Chinese University of Hong Kong, and the S.M. and Ph.D. degrees in electrical engineering from the Massachusetts Institute of Technology (MIT), Cambridge, in 1989 and 1993, respectively.

In the summer of 1990, he was a Researcher at the Schlumberger-Doll Research Center, where he worked on numerical modeling of acoustic logging in borehole structures. From 1988 to 1993, he was a Research Assistant at MIT. His research there included full-wave analyses of microwave integrated circuits and high speed interconnects, and numerical modeling of electromagnetic interference (EMI) and superconductor electromagnetics. He is currently Principal Engineer of Interconnect Analysis Technology, Viewlogic's Advanced Development Group (formerly Quad Design Technology), where he has developed algorithms for Viewlogic's EMI analysis products.

Dr. Lam is a member of Sigma Xi. He was a co-recipient of the best paper award at the 1996 IEEE International Symposium on EMC. He has served on the IEEE EMC/S TC-9 Computational EMC committee and the SAE EMC Modeling Task Force committee. He is listed in *Who's Who in Science and Engineering*, *Who's Who in America*, and *Who's Who in the World*.

**Lawrence Rubin** was born in the Bronx, NY, on November 20, 1953. He received the S.B.E.E. and S.M.E.E. degrees from the Massachusetts Institute of Technology, Cambridge, in 1974 and 1975, respectively.

From 1976 to 1984, he was employed at Hughes Aircraft Company, where he managed a department whose activities included the development of high performance signal processors, algorithm analysis, and the utilization of VHSIC technology for tactical electro-optical applications. From 1984 to 1986, he was Vice President for Advanced Development, Vitesse Electronics Corporation, where he served as Architect for a high performance parallel computer for scientific and signal processing applications. He is currently Group Vice President of Viewlogic's Advanced Development Group (formerly Quad Design Technology), where he has developed algorithms for timing verification, transmission line simulation, and field solutions used in the Advanced Development Group's CAE product line.